

Large Chern-Number Quantum Anomalous Hall Effect from Canted Antiferromagnetic Order in d -Electron System on Kagome Lattice

Waquar Ahmed,¹ Steffen Schäfer,¹ Pierre Lombardo,¹ Roland Hayn,¹ and Imam Makhfudz¹
¹IM2NP, UMR CNRS 7334, Aix-Marseille Université, 13013 Marseille, France

(Dated: 18 November 2025)

Electrons of d -symmetry interacting with a localized non-collinear antiferromagnetic spin order on a kagome lattice are considered. Even in the absence of an external magnetic field, spin-orbit coupling or relativistic effects, the spin texture produces a non-trivial intrinsic Berry curvature. This opens the route for a quantum anomalous Hall effect in the d -system. For spin orders with an out-of-plane component, the scalar spin chirality is finite, and the integration of the Berry curvature over the Brillouin zone may yield integer Hall conductivities in units of e^2/h . This canted configuration gives rise to the maximal possible Chern number, $C = \pm 5$ when the Fermi level is within nontrivial gap. The effect is best understood for – but not limited to – isotropic d -electron hopping and degenerate d -levels. In this case, analytic expressions are available and point to a topological origin for the manifestation of the maximal C . Numerical calculations show that these findings are robust to some anisotropy in the hopping integrals and to moderate splittings of the d levels. The $C = \pm 5$ plateau can be split into Chern peaks with smaller integers by varying the onsite energies. The topological phase transition between Hall plateaus of opposite C can be driven by flipping the out-of-plane component of the spin order, alluding to the potential of this system to quantum information.

Introduction. — The Anomalous Hall Effect (AHE), where an electric current produces a transverse voltage due to time-reversal symmetry breaking without external magnetic field, has been at the forefront of condensed matter physics, both due to its theoretical interest and the potential applications in dissipationless electronics.¹

Millennial-era advances in condensed matter physics are marked by the discovery of materials with electronic structures hosting peculiar features such as Dirac points and flatbands.^{2–5} When magnetism is present, such materials may form a frustration-induced quantum spin-liquid,^{6,7} or magnetically ordering may give rise to an AHE. The latter can be driven by extrinsic mechanisms such as impurities or disorder. However, a more fundamental perspective puts forward an AHE in clean systems, solely relying on phenomena inside the material itself such as e.g. an internal magnetic texture^{8–15,18,19} or an the effective magnetic field in reciprocal space (Berry curvature).^{20–22} The latter gives rise to the quantum anomalous Hall effect (QAHE)²³ characterized by an integer^{1,24} — the Chern number. Its occurrence was theoretically predicted in various systems,^{25–31} some of which were experimentally confirmed.^{32,33} A recent work of ours shows a QAHE for the d -electrons on a kagome lattice with ferromagnetic order.³⁴

A key ingredient of both, ordinary and quantum AHE, is the breaking of time-reversal symmetry. The latter is guaranteed in ferromagnets by a non-zero net magnetization. In antiferromagnets, by contrast, the net magnetization vanishes, and the ordering is not controllable by an applied magnetic field. This has led to the conventional belief that antiferromagnets are not suitable for applications. This view has been challenged by recent developments, demonstrating that some effects may still be explored, thus giving rise to new fields like antiferromagnetic spintronics³⁵.

It is well understood that in collinear bipartite antiferromagnets, e.g. on the honeycomb lattice, spin staggering implies a zero net magnetization and a spin-degenerate electronic structure. However, a zero net

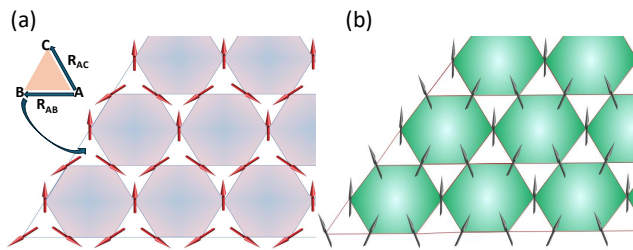


FIG. 1. (a) Coplanar non-collinear spin order with three sublattices carrying spins at 120° from each other. (b) Non-coplanar version obtained by adding an out-of-plane component to the spin order. The spins on the three sublattices are related to each other by 120° rotations around the center of the white triangle in the unit cell.

magnetization may also arise less trivially by non-collinear ordering, for example on triangular and kagome lattices.³⁶ On an antiferromagnetic kagome lattice, the ordinary AHE has been predicted theoretically from spin-orbit coupling¹⁵ and observed experimentally via its anomalously large Hall conductivity.^{16,17} Canted ferromagnetic and antiferromagnetic orders near collinearity, but with spin chirality, have been predicted to give rise to the chiral Hall effect³⁷ which was observed experimentally in van-der-Waals materials with non-coplanar spin order.³⁸

In heterostructured kagome systems, the QAHE due to canted spin order of localized d -orbital electrons has been studied theoretically for s -orbital conduction electrons.³⁹ In transition-metal based compounds, however, the conduction electrons are d -type, and the fate of the QAHE in such multi-orbital systems is still unclear. A natural question is therefore whether the QAHE can occur in a multi-orbital d -electron system with non-collinear spin order but *in absence* of spin-orbit coupling (SOC), since the orbital degree of freedom might either disrupt or reinforce the QAHE. The coupling of the localized spin texture to the conduction electrons may induce a spin-dependent effective flux in real space, as

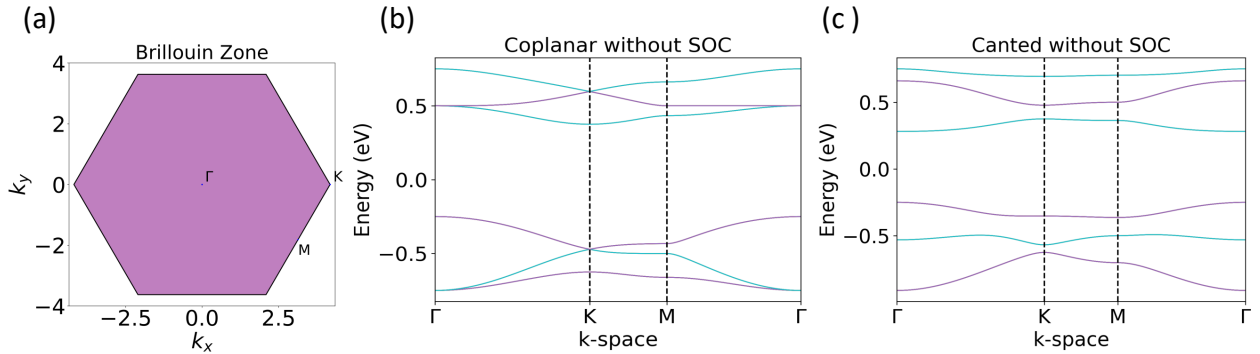


FIG. 2. (a) First Brillouin zone of the Kagome lattice, with points Γ , K and M . (b),(c) Band structures along the path $\Gamma - K - M - \Gamma$ for the hamiltonian (1), with isotropic hopping, and spin splitting arising due to non-collinear spin order. (b) Coplanar non-collinear spin order, with a large trivial gap around $E = 0$. (c) Non-coplanar spin order, with a large trivial gap and four small nontrivial gaps. Parameters: $E_1 = E_2 = E_3 = 0$ eV, $V_{dd\pi} = V_{dd\delta} = V_{dd\sigma} = -0.25$ eV, and $\mathbf{M}(\mathbf{r}) = (M_x(\mathbf{r}), M_y(\mathbf{r}), M_z(\mathbf{r})) = M_s(\sin \theta_{\mathbf{r}} \cos \phi_{\mathbf{r}}, \sin \theta_{\mathbf{r}} \sin \phi_{\mathbf{r}}, \cos \theta_{\mathbf{r}})$, with $M_s = 1$ eV, azimuthal angles $\phi_{\mathbf{r}} = 120^\circ$, and polar angles $\theta_{\mathbf{r}} = 90^\circ$ and $\theta_{\mathbf{r}} = 53^\circ$, in (b) and (c) respectively.

manifest in complex hopping integrals for the electrons and the spin splitting of the electronic structure, even without net magnetization. Coplanar non-collinear spin order turns out to give no QAHE due to trivial real space fluxes, unless transfer-type spin-orbit coupling is introduced.¹⁵

The topological QAHE requires non-coplanar non-collinear spin order. Here, we demonstrate this theoretically in a multi-orbital system, where all five d -orbitals contribute to the Chern number, but each spin sector with opposite sign. Under certain conditions this give a maximal Chern number of $C = \pm 5$ — the largest Chern number known presently to occur in natural quantum materials without heterostructuring.

Model. — We consider a minimal tight-binding model where the d -electrons are subject to orbital-dependent onsite energies (1st term), hopping (2nd term), and couple to the local spin order via a Zeeman exchange (3rd term) :

$$H = \sum_i E_\alpha d_{i,\alpha\sigma}^\dagger d_{i,\alpha\sigma} + \frac{1}{2} \sum_{\langle ij \rangle} \sum_{\alpha\alpha'\sigma} \left[t_{ij,\alpha\alpha'} d_{i,\alpha\sigma}^\dagger d_{j,\alpha'\sigma} + \text{h.c.} \right] - \sum_i d_{i,\alpha\sigma}^\dagger (\mathbf{M}_i \cdot \mathbf{s})_{\sigma,\sigma'} d_{i,\alpha\sigma'} \quad (1)$$

where $d_{i,\alpha\sigma}^\dagger (d_{i,\alpha\sigma})$ are creation (annihilation) operators for d -electrons of spin σ in orbital α and on site i as illustrated in Fig. 1. Although the onsite energies may be different for all five d -orbitals⁴¹, we consider the special case where only three different values occur, namely E_1 for the d_{z^2} -orbital, E_2 for d_{xz} and d_{yz} , and E_3 for d_{xy} and $d_{x^2-y^2}$, with the remaining degeneracies expressing lattice symmetries. The hopping elements $t_{ij,\alpha\alpha'}$ in the 2nd term are linear functions of the Slater-Koster integrals $V_{dd,\tau=\sigma,\pi,\delta}$ between two d orbitals⁴⁰. This makes the d -electron hopping orbital and direction dependent, and allows for an exchange between states belonging to different orbitals⁴¹. The Zeeman coupling in the third term results in a spin splitting due to an exchange with the local spin order. The corresponding magnetic moments for the sublattices are $\mathbf{M}_{i \in A,B,C}$, and their planar projection is assumed to be at 120° with respect to each other.

As illustrated in Fig. 1, the net magnetization M_z is zero for the coplanar case, but non-zero for a non-coplanar or canted spin order due to the out-of-the-plane component the spins. We will see below that the non-collinear magnetic structure gives rise to a non-relativistic spin splitting.

Band Structure and non-relativistic spin splitting — The first step is to compute the band structure of our Hamiltonian (1). It consists of 30 electronic bands stemming from 3 sublattices, with 5 orbitals and 2 spin states each. Fourier transforming under periodic boundary conditions then yields the \mathbf{k} -space Hamiltonian.

The resulting band structures are displayed in Fig. 2, for both, non-collinear but coplanar spin order, and non-collinear non-coplanar order. The kinetic hopping terms have been chosen to have the highest symmetry, i.e. $V_{dd\sigma} = V_{dd\delta} = V_{dd\pi}$ in the Slater-Koster integrals. This gives the simplest band structure, with almost flat bands, and linear or quadratic Dirac crossing points.⁵ We will call this situation the ‘isotropic limit’. Real materials usually have anisotropic Slater-Koster integrals, but we will show that the isotropic limit is a good reference point, and that our main results from the isotropic limit are preserved even away from this idealized case.

Fig. 2(b) shows that the coplanar non-collinear spin order splits the spin up and down bands. This marks the distinction between coplanar non-collinear spin order in a frustrated geometry like the kagome lattice, and collinear antiferromagnetic order on bipartite lattices: despite vanishing net magnetization in both cases, the latter shows no spin-splitting, and the bands remain two-fold spin degenerate; the coplanar non-collinear spin order, by contrast, lifts this Kramers degeneracy.

Canted spin ordering gives rise to a very neat band structure showing simultaneously a big trivial gap and significant non-trivial gaps (e.g. $\Delta E \sim 100 \dots 150$ meV for $M_s = 1$ eV), as illustrated in Fig. 2(c).⁴² The big trivial gap well separates the two spin sectors and allows for spin-polarized states, whereas placing the Fermi level in one of the smaller non-trivial gaps may give rise to topological insulating states like the Chern insulator. Spin canting therefore induces a spin

splitting which neither depends on relativistic effects nor on the distinction between different d -orbitals. It thus preserves the full orbital degeneracy and yields a simple band structure, making canted spin order a promising candidate in the quest for new topological phases of matter.

Real and Momentum Space Effective Magnetic Fluxes —

The non-collinear spin order gives rise to an effective magnetic flux felt by the electron⁴³ via a gauge field defined along the nearest-neighbor bond a_{ij} ,

$$\Phi_{\Delta,\nabla} = \sum_{ij \in \Delta,\nabla} a_{ij} \equiv \oint \mathbf{a} \cdot d\mathbf{r} = \int d\mathcal{S} \cdot (\nabla \times \mathbf{a}), \quad (2)$$

where the sum is over nearest neighbors around an up or down triangle, the \mathbf{a} vector is the continuous form of the gauge field, $d\mathbf{r}$ defines the path along the triangle, and \mathcal{S} is the surface normal vector. The local spin $\mathbf{S}_r = S(\sin \theta_r \cos \phi_r, \sin \theta_r \sin \phi_r, \cos \theta_r)$ corresponds to the magnetic moment \mathbf{M} in Eq. (1). A computation for spin- $\frac{1}{2}$ coherent states⁴⁴, appropriate for electrons, gives the gauge field¹⁹

$$a_{rr'} = -\arctan \left[\frac{\sin(\phi_{r'} - \phi_r) \sin \frac{\theta_r}{2} \sin \frac{\theta_{r'}}{2}}{\cos \frac{\theta_r}{2} \cos \frac{\theta_{r'}}{2} + \cos(\phi_{r'} - \phi_r) \sin \frac{\theta_r}{2} \sin \frac{\theta_{r'}}{2}} \right] \quad (3)$$

where $\mathbf{r} = (x_i, y_i)$, $\mathbf{r}' = (x_j, y_j)$, denotes the position vector of a lattice site and $a_{ij} \equiv a_{rr'}$. For coplanar non-collinear spin order with inter-spin angle 120° , $\theta_r = \theta_{r'} = \pi/2$ and $\phi_{r'} - \phi_r = 2\pi/3$, the gauge field simplifies to $a_{rr'} = -\pi/3$, thus giving the trivial fluxes $\Phi_{\Delta,\nabla} = -\pi$ of the time-reversal invariant phase with $\exp(i\pi) = \exp(-i\pi)$.¹² This result suggests that coplanar non-collinear spin order alone is not sufficient to produce a nontrivial flux that breaks time-reversal symmetry.

Non-coplanar spin order, by contrast, easily gives nontrivial fluxes, $\Phi_{\Delta,\nabla} \neq 0, \pm\pi$: still for the aforementioned $\phi_{r'} - \phi_r = 2\pi/3$, but with some finite $\theta_r = \theta_0$ for all sites, we obtain

$$a_{rr'} = -\arctan \left[\frac{\sqrt{3} \tan^2 \frac{\theta_0}{2}}{2 - \tan^2 \frac{\theta_0}{2}} \right].$$

This gauge field gives a nontrivial effective flux that can be associated with scalar spin chirality⁴⁵⁴⁶

$$\chi = \mathbf{S}_i \cdot (\mathbf{S}_j \times \mathbf{S}_k) = -\frac{3}{2} \sqrt{3} S^3 \cos \theta_0 \sin^2 \theta_0, \quad (4)$$

where i, j, k are the clockwise labels of three spins on a triangle, and $\theta_i = \theta_0$ on all three sublattices. From the scalar triple product structure, it is clear that the spin chirality vanishes for coplanar non-collinear antiferromagnetic spin order ($\theta_0 = \pi/2$), as well as for ferromagnetic order ($\theta_0 = 0, \pi$). Interestingly, the scalar spin chirality χ simply changes its sign when the canting is flipped; mirror-reflected with respect to the plane. That is, $\theta_0 \rightarrow \pi - \theta_0$ amounts to the same chirality with opposite sign. Two-fold degenerate states with related topological character but opposite chiralities are thus expected.

For the QAHE, the Hall conductivity is quantized in terms of an integer known as the Chern number C . The latter

is a topological invariant of the band structure, which can be computed from the Berry curvature $\Omega(\mathbf{k})$ in momentum space^{22,24}. For finite temperature T^1

$$\Omega(\mathbf{k}) = \hbar^2 \sum_{n \neq n'} G_{nn'}(\mathbf{k}) \text{Im} \left[\frac{\langle \psi_{n\mathbf{k}} | v_x(\mathbf{k}) | \psi_{n'\mathbf{k}} \rangle \langle \psi_{n'\mathbf{k}} | v_y(\mathbf{k}) | \psi_{n\mathbf{k}} \rangle}{(\varepsilon_{n'\mathbf{k}} - \varepsilon_{n\mathbf{k}})^2} \right] \quad (5)$$

with $G_{nn'}(\mathbf{k}) = f(\varepsilon_{n\mathbf{k}}) - f(\varepsilon_{n'\mathbf{k}})$, the Fermi function $f(\varepsilon) = [\exp(\beta(\varepsilon - E_F)) + 1]^{-1}$, and $\beta = 1/k_B T$ the inverse temperature. $|\psi_{n\mathbf{k}}\rangle$ and $\varepsilon_{n\mathbf{k}}$ are the n^{th} eigenstate and energy of the \mathbf{k} -space Hamiltonian, and $\mathbf{v}(\mathbf{k}) = \frac{1}{\hbar} \nabla_{\mathbf{k}} H(\mathbf{k})$ is the velocity operator.

The Hall conductivity σ_{xy} is related to the integral of Berry curvature over the Brillouin zone

$$\sigma_{xy} = \frac{e^2}{h} \frac{1}{2\pi} \int_{\text{BZ}} d^2\mathbf{k} \Omega(\mathbf{k}) = \frac{\Phi_B}{2\pi}. \quad (6)$$

The reciprocal-space Berry phase Φ_B ,²² is the intrinsic origin of the quantization of the Hall conductivity, $\sigma_{xy} = \frac{e^2}{h} C$, in units of the quantum of conductance e^2/h .

QAHE from Canted Antiferromagnetic Order — We first examine the Berry curvature for the particular parameter set of Fig. 2(c) resulting in the most remarkable Hall conductance. As shown in Fig. 3, the Berry curvature forms a landscape in the Brillouin zone, and according to the location of the Fermi energy, peaks of $\Omega(\mathbf{k})$ are found in different regions. Direct comparison with Fig. 2(c) shows that these peak regions correspond to the locations where the nontrivial gaps are tightest and where the curvature of the band is largest.

Next, the Hall conductivity σ_{xy} in units of the quantum of conductivity e^2/h is computed numerically exactly from the full 30×30 Hamiltonian matrix using Eq.(5). As can be seen from Fig. 4, for Fermi energies within a band, σ_{xy} is not an integer multiple of the conductance quantum (e^2/h). Only if the Fermi energy lies within a gap, quantization arises, and the corresponding integer is called the Chern number C . For non-collinear coplanar spin order with isotropic Slater-Koster integrals, we find $C = 0$ everywhere. This persists in the anisotropic case since the net magnetization is zero.

In our model (1), nonzero C requires non-coplanar (canted) non-collinear spin order. In this case, a finite Chern number occurs, since canted spin order allows for nonzero scalar spin chirality. When all onsite energies are degenerate, a relatively large $C = \pm 5$ plateau is obtained. This plateau is five times higher than the Chern plateaus found in corresponding ferromagnetic kagome systems^{48,49}, since all five d -orbitals contribute equally to the total Chern number. As pointed out earlier, this requires nontrivial real-space fluxes $\Phi_{\Delta,\nabla} \neq 0, \pm\pi$, as provided by a canted order, but absent in the coplanar non-collinear antiferromagnetic and (collinear) ferromagnetic spin orders due to the trivial flux from the latter two cases. To our knowledge, this is so far the largest Chern number occurring naturally in kagome systems, in absence of relativistic effects⁵² or heterostructure engineering⁵³.

Fig. 4 also shows that the two spin sectors carry opposite Chern numbers. As already pointed out, this correspond to scalar spin chiralities (4) with polar angles θ_0 and $\pi - \theta_0$. By

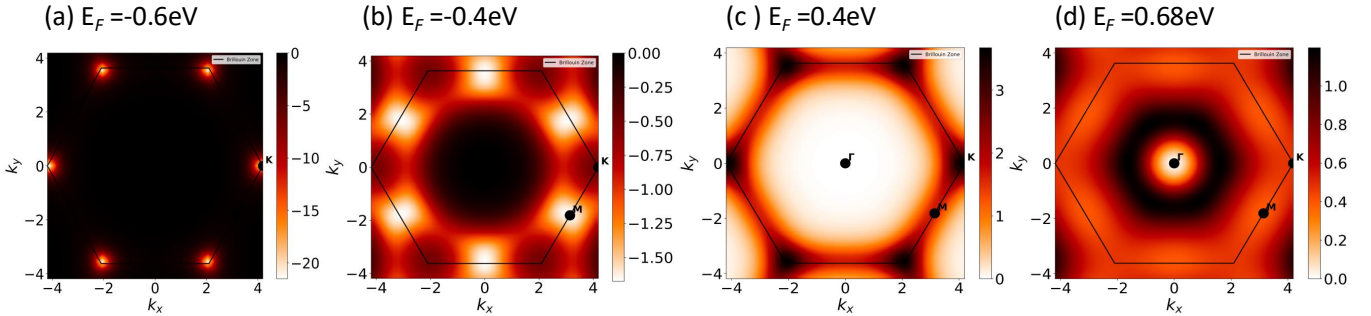


FIG. 3. Heat maps of the dimensionless Berry curvature $\Omega(k_x, k_y)$ for the parameter set of Fig. 2(c). The Fermi energy lies within the non-trivial gaps of the band structure, and is located in the spin-up sector for (a) and (b), and in the spin-down sector for (c) and (d).

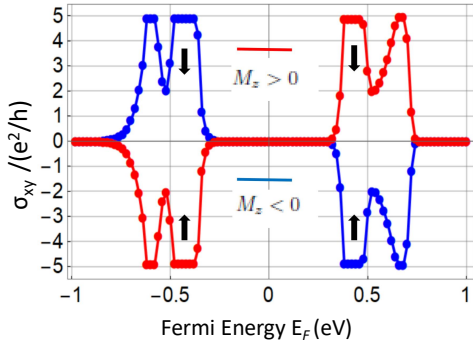


FIG. 4. Dimensionless Hall conductivity $\sigma_{xy}/(e^2/h)$ as a function of the Fermi energy E_F for $T = 0.1 \text{ meV} = 1.1 \text{ K}$ for 120° canted (non-coplanar) antiferromagnetic order. Parameters as in Fig. 2(c), with $M_z = 0.6 \text{ eV}$ (red) and $M_z = -0.6 \text{ eV}$ (blue), thus illustrating the symmetry. For some E_F , plateaus are found at the maximal Chern number $C = \pm 5$. The dots correspond to numerical data while the solid lines are guide to the eyes. The arrows mark the spin sectors.

tuning the Fermi energy or the filling factor, one can switch on or off one of the two counter-propagating chiral edge states of a given spin state, and thus realize half of the edge states of the quantum spin Hall effect⁵⁰ in two dimensions.

Low-Energy Theory and Topological Transition.— To gain conceptual insight beyond numerics, in particular on how such large Chern numbers as $|C| = 5$ may arise, we derive a low-energy effective theory for the d -electrons around the Dirac point, which in absence of spin order, the latter is located at K in the first Brillouin zone. An expansion for small $\mathbf{q} = \mathbf{k} - \mathbf{K}$ yields an effective massive Dirac Hamiltonian⁴¹

$$h_{\text{MD}}(\mathbf{q}) = \sigma_0 [h(\mathbf{K}) + v_F^x q_x J_x + v_F^y q_y J_y] - \frac{\hbar}{2} \boldsymbol{\sigma} \cdot \mathbf{M}_J. \quad (7)$$

The first contribution alone would be massless, and $\mathbf{v}_F = (\frac{\sqrt{3}t}{8}, \frac{3t}{8})$ represents the bare Fermi velocity vector of this theory. Mass is subsequently introduced by the Zeeman coupling in the second term.

$$h(\mathbf{K}) = \frac{t}{2} \begin{pmatrix} 0 & -1 & +1 \\ -1 & 0 & +1 \\ +1 & +1 & 0 \end{pmatrix} \quad (8)$$

is a constant matrix corresponding to the hamiltonian without spin order at the K -point, with $t = V_{dd\sigma} = V_{dd\delta} = V_{dd\pi}$ in the isotropic limit.

$$\mathbf{J}_x = \begin{pmatrix} 0 & -2 & -1 \\ -2 & 0 & -1 \\ -1 & -1 & 0 \end{pmatrix}, \quad \mathbf{J}_y = \begin{pmatrix} 0 & 0 & +1 \\ 0 & 0 & -1 \\ +1 & -1 & 0 \end{pmatrix}. \quad (9)$$

are matrices defined in the sublattice A, B, C space. In the Zeeman-like term, $\boldsymbol{\sigma}$ is the vector of Pauli spin matrices, and \mathbf{M}_J the sublattice magnetization,

$$\mathbf{M}_J = (M_J^x, M_J^y, M_J^z) = \left(\frac{\sqrt{3}}{2} M_\perp [J_A - J_B], M_\perp [J_C - \frac{1}{2} (J_A + J_B)], J_0 M_z \right) \quad (10)$$

with $M_\perp = \sqrt{M_x^2 + M_y^2}$. The J_0, J_A, J_B, J_C are diagonal matrices defined in the sublattice space with matrix element $(J_0)_{ij} = \delta_{ij}$, $(J_A)_{ij} = \delta_{ij} \delta_{iA}$ and similarly for J_B, J_C .

To compute the Hall conductivity and Chern number from the low-energy Hamiltonian (7), we perform a unitary transformation which diagonalizes the sublattice part of the problem, and obtain a generic expression in spin space,⁵¹

$$[h_{\text{Dirac}}(\mathbf{q})]_{i\bar{j}} = \left[E_i(\mathbf{q}) \sigma_0 + V_i \sigma_\alpha d_\alpha^{\tilde{i}}(\mathbf{q}) \right] \delta_{i\bar{j}}, \quad (11)$$

where $\tilde{i}, \tilde{j} = 1, 2, 3$ indicate matrix elements in the diagonal sublattice space, and $\mathbf{d}^{\tilde{i}}(\mathbf{q})$ is a directional vector with components $\alpha = x, y, z$. A detailed analysis gives

$$\mathbf{d}^{\tilde{i}}(\mathbf{q}) = \left(d_x^{\tilde{i}}(\mathbf{q}), d_y^{\tilde{i}}(\mathbf{q}), -\frac{\hbar}{2} M_z \right),$$

where the first two components depend evenly, but in a rather complicated manner, on M_z .⁴¹

Topological considerations show that the Chern number can now be expressed as

$$C = -\frac{1}{4\pi} \int_{\text{IBZ}} d^2 \mathbf{q} \hat{\mathbf{d}}^{\tilde{i}}(\mathbf{q}) \cdot \left[\frac{\partial \hat{\mathbf{d}}^{\tilde{i}}(\mathbf{q})}{\partial q_x} \times \frac{\partial \hat{\mathbf{d}}^{\tilde{i}}(\mathbf{q})}{\partial q_y} \right], \quad (12)$$

with hats denote unit vectors.⁵¹ Note that $d_z^{\tilde{i}}(\mathbf{q}) = -\frac{\hbar}{2} M_z$ does not depend on \mathbf{q} , such that

$$C = -\frac{1}{4\pi} \int_{\text{IBZ}} d^2 \mathbf{q} d_z^{\tilde{i}}(\mathbf{q}) \left[\frac{\partial d_x^{\tilde{i}}(\mathbf{q})}{\partial q_x} \frac{\partial d_y^{\tilde{i}}(\mathbf{q})}{\partial q_y} - \frac{\partial d_y^{\tilde{i}}(\mathbf{q})}{\partial q_x} \frac{\partial d_x^{\tilde{i}}(\mathbf{q})}{\partial q_y} \right],$$

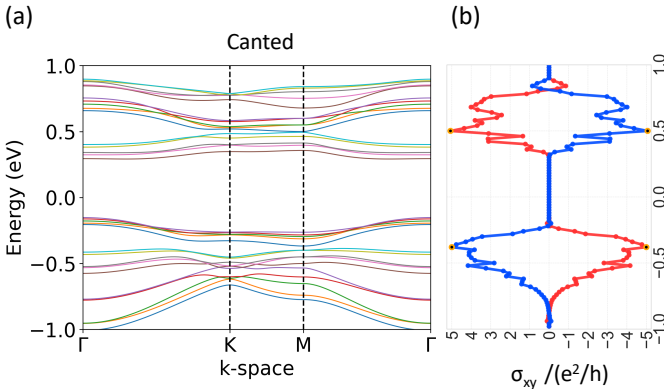


FIG. 5. Band structure (a) and Hall conductivity (b) at $T = 0.1 \text{ meV} = 1.1 \text{ K}$ for a kagome d -electron system with 120° canted antiferromagnetic order, with parameters (in eV) $E_1 = 0$, $E_2 = 0.05$, $E_3 = 0.10$, $V_{dd\pi} = -0.25$, $V_{dd\delta} = -0.35$, $V_{dd\sigma} = -0.15$, and $M_z = 1$, $M_z = \pm 0.6$ for the red/blue curves. Although far from the isotropic case, these parameters still give the maximum value $C = \pm 5$.

suggesting that the Chern number C should change sign with M_z ⁴¹ — an analytical result that perfectly agrees with the numerics presented in Fig. 4, thus indicating a topological phase transition in terms of the sign change of C when M_z is flipped.

The explicit dependence of the Chern number on an appropriately defined effective gap can be obtained by adapting results from the semiclassical Boltzmann equation and the Kubo formalism⁵⁴; for each d -orbital, we thus obtain

$$C = \left[\frac{\Delta}{\sqrt{\Delta^2 + 4\hbar^2 \left((\tilde{v}_F^x q_x)^2 + (\tilde{v}_F^y q_y)^2 \right)}} \right]_{\mathbf{q}=\mathbf{q}_F} = \text{sign}(\Delta).$$

Taking the Fermi wave-vector \mathbf{q}_F at its bare value, *i.e.* the Dirac point of the massless theory at K , reduces the expression in brackets to just a sign function. The calculated gap remains of constant sign in each Bloch hemisphere but changes in sign when crossing the equator $\theta = \pi/2$, thus further confirming the conclusion from the topological consideration described earlier.⁴¹

For θ close to the equator, a simple expression for the real-space spin Berry phase from a continuum formula can be obtained:⁴⁴ $\Phi = s \oint d\tau \dot{\phi} (1 - \cos \theta) = \pi(1 - \cos \theta)$ for $s = 1/2$. This asymptotically reproduces $\Phi_{\Delta, \nabla}$ of Eqs.(2) and (3) in the limit of $|\tan \theta| \rightarrow \infty$. Applying the result from the flux model¹² for Fermi energies within a nontrivial gap, the Chern number for the kagome lattice with degenerate onsite energies for all five d -orbitals is given by

$$C = \pm 5 \text{sign}[\sin \pi(1 - \cos \theta)]. \quad (13)$$

Robustness of the large Chern numbers in the non-degenerate anisotropic case.— While the result from Eq.(13) relies on the five-fold degeneracy of the d -orbitals, it is still supposed to hold if this degeneracy is lifted, under

the assumption that there is a remaining overlap between the observed gaps and the non-trivial gaps of the 5-fold degenerate limit. This prediction is confirmed by our numerical calculations which yield maximal Chern numbers $C = \pm 5$ even in the non-degenerate case. This robustness is an important result, since it implies that fine tuning of the parameters is not required.

We compute σ_{xy} for various sets of parameters involving slightly different onsite energies and anisotropic Slater-Koster integrals, such that the hopping parameters $t_{ij,\alpha\alpha'}$ in the second term of Eq.(1) acquire an orbital and direction dependence. This process, in turn, leads to a "Wigner rotation" of the d -orbitals, the details of which are given in⁴¹.

The corresponding band structure and Hall conductivity is shown in Fig. 5. Quantifying the anisotropy as $|(V_{dd\delta} - V_{dd\pi})/(2V_{dd\pi})|$, the parameter set involves 40% anisotropy in the Slater-Koster integrals and non-degenerate onsite energies (apart from degeneracy between symmetry-related d -orbitals, *e.g.* d_{xz}, d_{yz}). The plot shows 30 energy bands, thus indicating a complete lifting of the degeneracies except, of course, at the crossing points. We find that the maximal $C = \pm 5$ to persist away from the isotropic and degenerate cases, and even for anisotropies up to 80%⁴¹, implying a surprising robustness.

Finally, we study the effect of increasing differences in the onsite energies, which produce simple shifts of the $C = \pm 1$ contribution in each orbital. In real materials, where the onsite energies may differ from orbital to orbital, this, in principle, allows for all possibilities between $C = -5$ and $+5$. Therefore, the Chern numbers may still sum up to the maximal $C = \pm 5$. This upper bound for a Chern number in a d -electron system is not attainable in ferromagnetically ordered³⁴ or coplanar non-collinear systems [see Figs. 1(a) and 2(b)]. Therefore, the predicted large Chern QAHE is unique to canted spin order, in d -electron systems that do not involve any spin-orbit coupling.

Discussion and Conclusions.— We investigate the quantum anomalous Hall effect of the d -electrons due to canted antiferromagnetic order on a kagome lattice. In this case, the required spin splitting in the electronic band structure comes from the real-space effective field induced by the spin order with finite scalar spin chirality. In a sense, the predicted phenomenon is a quantum and antiferromagnetic version of the topological Hall effect, originally proposed in classical systems with ferromagnetic order.¹⁸ One important finding is the robustness of the predicted maximal Chern numbers in the canted spin configuration. The maximal C persists in presence of orbital-dependent hopping parameters and a moderate lifting of d -level degeneracy, which makes it relevant for real materials. Pairs of Chern plateaus with opposite signs emerge from spin-momentum locking, and C and M_z change sign simultaneously, due to spin chirality. The canted spin order enables equal contribution from all the five d -orbitals, resulting in quantum anomalous Hall effect with large Chern numbers that can be tuned by varying the onsite energies.

Acknowledgements.— I.M. thanks M. Diouf, N. and R. Saidi, M. Ngom, C. Ngbo-Tiba Guiguisia, and M. Beye for the numerous discussions during their internship which

inspired the author to pursue and complete this work. W.A. acknowledges the doctoral funding from Aix-Marseille Université that financially supports the author in this research. I.M. conceived the idea and the plan for the project. W.A., I.M., S.S., and R.H. performed the numerical calculations, while I.M. and P.L. derived the analytical results. All authors were involved in the analysis of the results and the writing of the manuscript.

- ¹N. Nagaosa, J. Sinova, S. Onoda, A. H. MacDonald, and N. P. Ong, Anomalous Hall effect, *Rev. Mod. Phys.* 82, 1539 (2010).
- ²T. Neupert, L. Santos, C. Chamon, and C. Mudry, Fractional Quantum Hall States at Zero Magnetic Field, *Phys. Rev. Lett.* 106, 236804 (2011).
- ³K. Sun, Z. Gu, H. Katsura, and S. Das Sarma, Nearly-flat bands with nontrivial topology, *Phys. Rev. Lett.* 106, 236803 (2011).
- ⁴E. Tang, J.-W. Mei, and X.-G. Wen, High temperature fractional quantum Hall states, *Phys. Rev. Lett.* 106, 236802 (2011).
- ⁵M. Kang, L. Ye, S. Fang, J.-S. You, A. Levitan, M. Han, J. I. Facio, C. Jozwiak, A. Bostwick, E. Rotenberg, M. K. Chan, R. D. McDonald, D. Graf, K. Kaznatcheev, E. Vescovo, D. C. Bell, E. Kaxiras, J. van den Brink, M. Richter, M. P. Ghimire, J. G. Checkelsky, and R. Comin, Dirac fermions and flat bands in the ideal kagome metal FeSn, *Nat. Mater.* 19, 163 (2020).
- ⁶I. Makhfudz, Fluctuation-induced First Order Quantum Phase Transition of U(1) Quantum Spin Liquid in Pyrochlore Quantum Antiferromagnet, *Phys. Rev. B* 89, 024401 (2014).
- ⁷L. Savary and L. Balents, Quantum Spin Liquids, *Rep. Prog. Phys.* 80, 016502 (2017).
- ⁸Taguchi Y, Oohara Y, Yoshizawa H, Nagaosa N, and Tokura Y, Spin Chirality, Berry Phase, and Anomalous Hall Effect in a Frustrated Ferromagnet, *Science* 291(5513), 2573 (2001).
- ⁹J. Ye, Y. B. Kim, A. J. Millis, B. I. Shraiman, P. Majumdar, and Z. Tešanović, Berry phase theory of the Anomalous Hall Effect: Application to Colossal Magnetoresistance Manganites, *Phys. Rev. Lett.* 83, 3737 (1999).
- ¹⁰S. Onoda and N. Nagaosa, Spin Chirality Fluctuation and Anomalous Hall Effect in Itinerant Ferromagnets, *Phys. Rev. Lett.* 90, 196602 (2003).
- ¹¹I. Martin and C. D. Batista, Scalar spin chirality and quantum Hall effect on triangular lattice, *Phys. Rev. Lett.* 101, 156402 (2008).
- ¹²Ohgushi K., Murakami S., Nagaosa N., Spin Anisotropy and Quantum Hall Effect in the Kagome Lattice - Chiral Spin State based on a Ferromagnet, *Phys. Rev. B* 62, R6065 (2000).
- ¹³Z. Fang, N. Nagaosa, K. S. Takahashi, A. Asamitsu, R. Mathieu, T. Ogasawara, H. Yamada, M. Kawasaki, Y. Tokura, and K. Terakura, The Anomalous Hall Effect and Magnetic Monopoles in Momentum Space, *Science* 302, 92 (2003).
- ¹⁴M. Taillefumier, B. Canals, C. Lacroix, V. K. Dugaev, and P. Bruno, Anomalous Hall effect due to spin chirality in the Kagomé lattice, *Phys. Rev. B* 74, 085105 (2006).
- ¹⁵H. Chen, Q. Niu, and A. H. MacDonald, Anomalous Hall Effect Arising from non-collinear Antiferromagnetism, *Phys. Rev. Lett.* 112, 017205 (2014).
- ¹⁶A. K. Nayak, J. E. Fischer, Y. Sun, B. Yan, J. Karel, A. C. Komarek, C. Shekhar, N. Kumar, W. Schnelle, J. Kubler, C. Felser, and S. S. P. Parkin, Large anomalous Hall effect driven by a nonvanishing Berry curvature in the noncollinear antiferromagnet Mn₃Ge, *Sci. Adv.* 2, e1501870 (2016).
- ¹⁷S. Nakatsuji, N. Kiyohara, and T. Higo, Large anomalous Hall effect in a non-collinear antiferromagnet at room temperature, *Nature (London)* 527, 212 (2015).
- ¹⁸P. Bruno, V. K. Dugaev, and M. Taillefumier, Topological Hall Effect and Berry Phase in Magnetic Nanostructures, *Phys. Rev. Lett.* 93, 096806 (2004).
- ¹⁹I. Makhfudz and P. Pujol, Protection against Spin Gap in 2-d Insulating Antiferromagnets with a Chern-Simons Term, *Phys. Rev. B* 92, 144507 (2015).
- ²⁰G. Sundaram and Q. Niu, Wave-packet dynamics in slowly perturbed crystals: Gradient corrections and Berry-phase effects, *Phys. Rev. B* 59, 14915 (1999).
- ²¹N. A. Sinitsyn, Semiclassical theories of the anomalous Hall effect, *J. Phys.: Cond. Matt.* 20 (2008) 023201.
- ²²F. D. M. Haldane, Berry Curvature on the Fermi Surface: Anomalous Hall Effect as a Topological Fermi-Liquid Property, *Phys. Rev. Lett.* 93, 206602 (2004).
- ²³C.-Z. Chang, C.-X. Liu, and A. H. MacDonald, Colloquium: Quantum anomalous Hall effect, *Rev. Mod. Phys.* 95, 011002 (2023).
- ²⁴D. J. Thouless, M. Kohmoto, M. P. Nightingale, and M. den Nijs, Quantized Hall Conductance in a Two-Dimensional Periodic Potential, *Phys. Rev. Lett.* 49, 405 (1982).
- ²⁵F. D. M. Haldane, Model for a Quantum Hall Effect without Landau Levels: Condensed-Matter Realization of the "Parity Anomaly", *Phys. Rev. Lett.* 61, 2015 (1988).
- ²⁶M. Onoda and N. Nagaosa, Quantized Anomalous Hall Effect in Two-Dimensional Ferromagnets: Quantum Hall Effect in Metals, *Phys. Rev. Lett.* 90, 206601 (2003).
- ²⁷K. Sun, H. Yao, E. Fradkin, and S. A. Kivelson, Topological Insulators and Nematic Phases from Spontaneous Symmetry Breaking in 2D Fermi Systems with a Quadratic Band Crossing, *Phys. Rev. Lett.* 103, 046811 (2009).
- ²⁸Z. Qiao, W. Ren, H. Chen, L. Bellaiche, Z. Zhang, A. H. MacDonald, and Q. Niu, Quantum Anomalous Hall Effect in Graphene Proximity Coupled to an Antiferromagnetic Insulator, *Phys. Rev. Lett.* 112, 116404 (2014).
- ²⁹P. Högl, T. Frank, K. Zollner, D. Kochan, M. Gmitra, and J. Fabian, Quantum Anomalous Hall Effects in Graphene from Proximity-Induced Uniform and Staggered Spin-Orbit and Exchange Coupling, *Phys. Rev. Lett.* 124, 136403 (2020).
- ³⁰C.-X. Liu, X.-L. Qi, X. Dai, Z. Fang, and S.-C. Zhang, Quantum Anomalous Hall Effect in Hg(1-y)Mn(y)Te Quantum Wells, *Phys. Rev. Lett.* 101, 146802 (2008).
- ³¹C.-X. Liu, S.-C. Zhang, and X.-L. Qi, The Quantum Anomalous Hall Effect: Theory and Experiment, *Annu. Rev. Condens. Matter Phys.* 7, 301 (2016).
- ³²C.-Z. Chang, J. Zhang, X. Feng, J. Shen, Z. Zhang, M. Guo, K. Li, Y. Ou, P. Wei, L.-L. Wang, Z.-Q. Ji, Y. Feng, S. Ji, X. Chen, J. Jia, X. Dai, Z. Fang, S.-C. Zhang, K. He, Y. Wang, L. Lu, X.-C. Ma, and Q.-K. Xue, Experimental Observation of the Quantum Anomalous Hall Effect in a Magnetic Topological Insulator, *Science* 340, 167 (2013).
- ³³Deng, Y., Yu, Y., Shi, M. Z., Guo, Z., Xu, Z., Wang, J., Chen, X.H., and Zhang, Y., Quantum anomalous Hall effect in intrinsic magnetic topological insulator MnBi₂Te₄, *Science* 367, 895 (2020).
- ³⁴I. Makhfudz, M. Cherkasskii, M. Alipourzadeh, Y. Hajati, P. Lombardo, S. Schäfer, S. V. Kusminskiy, and R. Hayn, Quantum anomalous Hall effect in *d*-electron kagome systems: Chern insulating states from transverse spin-orbit coupling, *Phys. Rev. B* 110, 235130 (2024).
- ³⁵V. Baltz, A. Manchon, M. Tsoi, T. Moriyama, T. Ono, and Y. Tserkovnyak, Antiferromagnetic spintronics, *Rev. Mod. Phys.* 90, 015005 (2018).
- ³⁶S. Sachdev, Kagome' - and triangular-lattice Heisenberg antiferromagnets: Ordering from quantum fluctuations and quantum-disordered ground states with unconfined bosonic spinons, *Phys. Rev. B* 45, 12377 (1992).
- ³⁷J. Kipp, K. Samanta, F. R. Lux, M. Merte, J.-P. Hanke, M. Redies, F. Freimuth, S. Blügel, M. Ležaić, Y. Mokrousov, The chiral Hall effect in canted ferromagnets and antiferromagnets, *Communications Physics* 4, 99 (2021).
- ³⁸H. Takagi, R. Takagi, S. Minami, T. Nomoto, K. Ohishi, M.-T. Suzuki, Y. Yanagi, M. Hirayama, N. D. Khanh, K. Karube, H. Saito, D. Hashizume, R. Kiyanagi, Y. Tokura, R. Arita, T. Nakajima, and S. Seki, Spontaneous topological Hall effect induced by non-coplanar antiferromagnetic order in intercalated van der Waals materials, *Nature Physics* 19, 961 (2023).
- ³⁹X. Zhou, W. Feng, Y. Li, Y. Yao, Spin-Chirality-Driven Quantum Anomalous and Quantum Topological Hall Effects in Chiral Magnets, *Nano Lett.* 23, 5680 (2023).
- ⁴⁰W. A. Harrison, *Electronic Structure and the Properties of Solids: The Physics of the Chemical Bond* (Dover Publications, Inc., New York, United States (1980)).
- ⁴¹Please see the supplementary materials containing the details of Slater-Koster integrals, the derivation of low-energy Dirac Hamiltonian, the role of anisotropy in Slater-Koster integrals, canting angle, and onsite energy. These materials also make reference to ^{12,34,40,51}.
- ⁴²Even though the non-collinear spin order mixes up spin up and spin down sectors, we will continue to use this phrase, implying in Fig. 2(b,c) the upper group of bands as spin down (up) sector and lower group of bands as spin up (down) sector for $M_z > 0 (< 0)$, just like in ferromagnetic case³⁴.

⁴³I. Makhfudz and P. Pujol, Hole properties on and off magnetization plateaus in 2D antiferromagnets, *Phys. Rev. Lett.* 114, 087204 (2015).

⁴⁴A. Auerbach, *Interacting Electrons and Quantum Magnetism* (Springer, New York, United States (1994)).

⁴⁵X. G. Wen, Frank Wilczek, and A. Zee, Chiral spin states and superconductivity, *Phys. Rev. B* 39, 11413 (1989).

⁴⁶I. Makhfudz, Effective field theory of chiral spin liquid between ordered phases in a kagome antiferromagnet, *J. Phys.: Condens. Matter* 30, 225801 (2018).

⁴⁷S. Okamoto, N. Mohanta, E. Dagotto, and D. N. Sheng, Topological flat bands in a kagome lattice multiorbital system, *Communications Physics* 5, 198 (2022).

⁴⁸G. Xu, B. Lian, and S-C. Zhang, Intrinsic Quantum Anomalous Hall effect in Kagome lattice Cs₂LiMn₃F₁₂, *Phys. Rev. Lett.* 115, 186802 (2015).

⁴⁹L. Ye, M. Kang, J. Liu, F. von Cube, C. R. Wicker, T. Suzuki, C. Jozwiak, A. Bostwick, E. Rotenberg, D. C. Bell, L. Fu, R. Comin, and J. G. Checkelsky, Massive Dirac fermions in a ferromagnetic kagome metal, *Nature* 555, 638 (2018).

⁵⁰C. L. Kane and E. J. Mele, Quantum Spin Hall Effect in Graphene, *Phys. Rev. Lett.* 95, 226801 (2005).

⁵¹Qi, X. L., Wu, Y.-S., and Zhang, S.-C., Topological quantization of the spin Hall effect in two-dimensional paramagnetic semiconductors, *Phys. Rev. B* 74, 085308 (2006).

⁵²J. Wang, B. Lian, H. Zhang, Y. Xu, and S-C. Zhang, Quantum Anomalous Hall Effect with Higher Plateaus, *Phys. Rev. Lett.* 111, 136801 (2013).

⁵³C. Fang, M. J. Gilbert, and B. A. Bernevig, Large-Chern-Number Quantum Anomalous Hall Effect in Thin-Film Topological Crystalline Insulators, *Phys. Rev. Lett.* 112, 046801 (2014).

⁵⁴N. A. Sinitsyn, A. H. MacDonald, T. Jungwirth, V. K. Dugaev, and J. Sinova, Anomalous Hall effect in a two-dimensional Dirac band: The link between the Kubo-Streda formula and the semiclassical Boltzmann equation approach, *Phys. Rev. B* 75, 045315 (2007).

Supplementary Materials: Large Chern-Number Quantum Anomalous Hall Effect from Canted Antiferromagnetic Order in d -Electron System on Kagome Lattice

W. Ahmed¹, S. Schäfer¹, P. Lombardo¹, R. Hayn¹, and I. Makhfudz¹

¹IM2NP, UMR CNRS 7334, Aix-Marseille Université, 13013 Marseille, France

In these Supplementary Materials, we provide additional details supplementing the main text. First, the details of the Slater-Koster integrals and their implementation in the Hamiltonian diagonalization are given. Next, the derivation of low-energy theory reported in the main text to discuss the topological phase transition is provided. Then, supplemental results on the roles of onsite energy, robustness of the predicted large-Chern number QAHE on the anisotropy in the Slater-Koster integrals, and the dependence of QAHE on the canting angle are presented.

I. SLATER-KOSTER INTEGRALS, THEIR IMPLEMENTATION, AND ORBITAL ROTATION

Different from s -electrons, which have no orbital degree of freedom, d -orbital electrons constitute an inherent multi-orbital system because of the orbital angular momentum, accompanying the spin angular momentum. A d -orbital electron thus carries orbital and spin angular momenta, characterized in terms of the corresponding quantum numbers $l = 2$ and spin $s = 1/2$. The Hamiltonian matrix corresponding to Eq.(1) in the main text is written in the basis states involving the five d -orbitals, three sublattices, and two spin states (up and down spin).

The five d -orbitals ($d_{xy}, d_{yz}, d_{z^2}, d_{xz}, d_{x^2-y^2}$) basis states correspond to real spherical harmonics Y_{l,m_l} with $l = 2$, which can be written in terms of complex spherical harmonics, on which the orbital angular momentum operator \mathbf{l} operates; the complex spherical harmonics correspond to the eigenfunctions of the orbital angular momentum $l_z|l,m_l\rangle = m_l\hbar|l,m_l\rangle$, $Y_l^{m_l}(x,y,z) \equiv \langle \theta, \phi |l, m_l \rangle$. The relations are given by

$$d_{xy} \equiv Y_{2,-2} = i\sqrt{\frac{1}{2}}(Y_2^{-2} - Y_2^2) \quad (14)$$

$$d_{yz} \equiv Y_{2,-1} = i\sqrt{\frac{1}{2}}(Y_2^{-1} + Y_2^1) \quad (15)$$

$$d_{z^2} \equiv Y_{2,0} = Y_2^0 \quad (16)$$

$$d_{xz} \equiv Y_{2,1} = \sqrt{\frac{1}{2}}(Y_2^{-1} - Y_2^1) \quad (17)$$

$$d_{x^2-y^2} \equiv Y_{2,2} = \sqrt{\frac{1}{2}}(Y_2^{-2} + Y_2^2) \quad (18)$$

where Y_{l,m_l} and $Y_l^{m_l}$ are real and complex spherical harmonics functions respectively. More generally, we can write

$$|d_\alpha\rangle \equiv Y_{2,m_l} = \sum_{m_l} c_{\alpha;m_l} Y_2^{m_l} \equiv \sum_{m_l} c_{\alpha;m_l} |2, m_l\rangle \quad (19)$$

where $\alpha = xy, yz, z^2, xz, x^2 - y^2$ while $c_{\alpha;m_l}$ is complex coefficient, which can be deduced from Eqs.(14-18).

The multi-orbital character of d -electron system manifests in the kinetic hopping term in its tight-binding Hamiltonian, Eq.(1) in the main text. The hopping constant $t_{ij,\alpha,\alpha'}$ depends on the orbitals $d_\alpha(d_{\alpha'})$ at the sites $i(j)$ respectively and is determined from Slater-Koster integrals. We write the nearest neighbor vectors as

$$\mathbf{r}_{ij} = a(l\hat{\mathbf{x}} + m\hat{\mathbf{y}} + n\hat{\mathbf{z}}), \quad (20)$$

where a is the lattice spacing, $\hat{\mathbf{x}}, \hat{\mathbf{y}}, \hat{\mathbf{z}}$ are unit vectors in x, y, z directions respectively. Eventually, we automatically have $n = 0$ in our two-dimensional system. The Slater-Koster hopping integrals are given as follows¹;

$$t_{xz;xz} = 3n^2l^2V_{dd\sigma} + (n^2 + l^2 - 4n^2l^2)V_{dd\pi} + (m^2 + n^2l^2)V_{dd\delta} \quad (21)$$

$$t_{xz,yz} = 3n^2lmV_{dd\sigma} + lm(1 - 4n^2)V_{dd\pi} + lm(n^2 - 1)V_{dd\delta} \quad (22)$$

$$t_{yz,yz} = 3m^2n^2V_{dd\sigma} + (m^2 + n^2 - 4m^2n^2)V_{dd\pi} + (l^2 + m^2n^2)V_{dd\delta} \quad (23)$$

$$t_{xy,xy} = 3l^2m^2V_{dd\sigma} + (l^2 + m^2 - 4l^2m^2)V_{dd\pi} + (n^2 + l^2m^2)V_{dd\delta} \quad (24)$$

$$t_{xy,x^2-y^2} = \frac{3}{2}lm(l^2 - m^2)V_{dd\sigma} + 2lm(m^2 - l^2)V_{dd\pi} + \frac{1}{2}lm(l^2 - m^2)V_{dd\delta} \quad (25)$$

$$t_{xy,z^2} = \sqrt{3}lm(n^2 - \frac{1}{2}(l^2 + m^2))V_{dd\sigma} - 2\sqrt{3}lmn^2V_{dd\pi} + \frac{\sqrt{3}}{2}lm(1 + n^2)V_{dd\delta} \quad (26)$$

$$t_{x^2-y^2,x^2-y^2} = \frac{3}{4}(l^2 - m^2)^2V_{dd\sigma} + (l^2 + m^2 - (l^2 - m^2)^2)V_{dd\pi} + (n^2 + \frac{1}{4}(l^2 - m^2)^2)V_{dd\delta} \quad (27)$$

$$t_{x^2-y^2,z^2} = \frac{\sqrt{3}}{2}(l^2 - m^2)(n^2 - \frac{1}{2}(l^2 + m^2))V_{dd\sigma} + \sqrt{3}n^2(m^2 - l^2)V_{dd\pi} + \frac{\sqrt{3}}{4}(1 + n^2)(l^2 - m^2)V_{dd\delta} \quad (28)$$

$$t_{z^2,z^2} = (n^2 - \frac{1}{2}(l^2 + m^2))^2V_{dd\sigma} + 3n^2(l^2 + m^2)V_{dd\pi} + \frac{3}{4}(l^2 + m^2)^2V_{dd\delta} \quad (29)$$

where $V_{dd\sigma}, V_{dd\pi}, V_{dd\delta}$ are the Slater-Koster integrals, while l, m, n are the Cartesian components of the nearest-neighbor vectors. The group of π -orbitals (d_{xz}, d_{yz} orbitals) and the group of σ -orbitals ($d_{xy}, d_{x^2-y^2}, d_{z^2}$ orbitals) are separate and do not have nonzero Slater-Koster integrals between the two groups. The kinetic hopping part of the Hamiltonian gives rise to matrix elements that can be directly extracted from Slater-Koster integrals, as available in¹.

One can see from Eqs.(21-29) that the Slater-Koster integrals connecting different d -orbitals depend on the types of the two orbitals and the direction of hopping between neighboring sites. Furthermore, since the Slater-Koster integrals between different orbital types are in general nonzero, the hopping involves an orbital rotation that converts (or reorientates) one orbital state to another orbital state. This is an intrinsic property of multi-orbital system like d -electron system that is absent in s -orbital electron system, where the orbital angular momentum is zero. This orbital rotation is driven by the hopping term and the rotation occurs as long as the Slater-Koster integrals V_{dd} 's are not all equal; when the three V_{dd} 's are equal, the kinetic hopping part of the Hamiltonian is diagonal in the orbital basis $t_{\alpha\alpha'} = t\delta_{\alpha\alpha'}$ and there is no orbital rotation.

II. DERIVATION OF EFFECTIVE LOW-ENERGY HAMILTONIAN

We start from the kinetic part of the Hamiltonian in Fourier space, which takes the form of a 3×3 matrix defined in the sublattice space;

$$h(\mathbf{k}) = t \begin{pmatrix} 0 & \cos \mathbf{k} \cdot \mathbf{d}_{AB} & \cos \mathbf{k} \cdot \mathbf{d}_{CA} \\ \cos \mathbf{k} \cdot \mathbf{d}_{AB} & 0 & \cos \mathbf{k} \cdot \mathbf{d}_{BC} \\ \cos \mathbf{k} \cdot \mathbf{d}_{CA} & \cos \mathbf{k} \cdot \mathbf{d}_{BC} & 0 \end{pmatrix} \quad (30)$$

where $t = V_{dd\sigma} = V_{dd\delta} = V_{dd\pi}$ in isotropic limit and $\mathbf{d}_{AB}, \mathbf{d}_{BC}, \mathbf{d}_{CA}$ are nearest-neighbor unit vectors between two adjacent sites (or sublattices). Expanding the Hamiltonian around Dirac point, $\mathbf{k} = \mathbf{K} + \mathbf{q}$, we obtain

$$h(\mathbf{k}) = h(\mathbf{K}) + h(\mathbf{q}) \quad (31)$$

where $h(\mathbf{K})$ is a constant Hamiltonian defined at \mathbf{K} , where the Dirac point is located, and is fixed as a reference. The unit cell triangle and the three sublattices (and the spin vector orientation for the co-planar collinear spin order assumed) are illustrated in Fig. 6. Expanding the cosine term to linear order in \mathbf{q} , e.g. $\cos(\mathbf{K} + \mathbf{q}) \cdot \mathbf{d}_{AB} = \cos \mathbf{K} \cdot \mathbf{d}_{AB} \cos \mathbf{q} \cdot \mathbf{d}_{AB} - \sin \mathbf{K} \cdot \mathbf{d}_{AB} \sin \mathbf{q} \cdot \mathbf{d}_{AB} \approx \cos \mathbf{K} \cdot \mathbf{d}_{AB} - \mathbf{q} \cdot \mathbf{d}_{AB} \sin \mathbf{K} \cdot \mathbf{d}_{AB}$, we obtain

$$h(\mathbf{K}) = \frac{t}{2} \begin{pmatrix} 0 & -1 & 1 \\ -1 & 0 & 1 \\ 1 & 1 & 0 \end{pmatrix} \quad (32)$$

for the constant Hamiltonian part and

$$h(\mathbf{q}) = t \begin{pmatrix} 0 & -\mathbf{q} \cdot \mathbf{d}_{AB} s_{AB} & -\mathbf{q} \cdot \mathbf{d}_{CA} s_{CA} \\ -\mathbf{q} \cdot \mathbf{d}_{AB} s_{AB} & 0 & -\mathbf{q} \cdot \mathbf{d}_{BC} s_{BC} \\ -\mathbf{q} \cdot \mathbf{d}_{CA} s_{CA} & -\mathbf{q} \cdot \mathbf{d}_{BC} s_{BC} & 0 \end{pmatrix} \quad (33)$$

where we have introduced a shorthand notation $s_{AB} = \sin \mathbf{K} \cdot \mathbf{d}_{AB}$ and similarly for the other two pairs of sublattices. The vectors $\mathbf{d}_{AB}, \mathbf{d}_{BC}, \mathbf{d}_{CA}$ can be deduced from Fig. 6. We will use a convention where the length of the nearest-neighbor vector is 1/2 instead of 1 as used in². As such, the Dirac point is located at $\mathbf{K} = 4\pi/3$. The resulting linear in- \mathbf{q} part of the Hamiltonian becomes

$$h_{\text{Dirac}}(\mathbf{q}) = \frac{t}{2} \begin{pmatrix} 0 & -\frac{\sqrt{3}}{2} q_x & \frac{\sqrt{3}}{2} \left(-\frac{q_x}{2} + \frac{\sqrt{3}}{2} q_y \right) \\ -\frac{\sqrt{3}}{2} q_x & 0 & -\frac{\sqrt{3}}{2} \left(\frac{q_x}{2} + \frac{\sqrt{3}}{2} q_y \right) \\ \frac{\sqrt{3}}{2} \left(-\frac{q_x}{2} + \frac{\sqrt{3}}{2} q_y \right) & -\frac{\sqrt{3}}{2} \left(\frac{q_x}{2} + \frac{\sqrt{3}}{2} q_y \right) & 0 \end{pmatrix} \quad (34)$$

which can be simply written as

$$h_{\text{Dirac}}(\mathbf{q}) = \frac{\sqrt{3}}{8} t \left(q_x J_x + \sqrt{3} q_y J_y \right) \quad (35)$$

where the J matrices are given by

$$J_x = \begin{pmatrix} 0 & -2 & -1 \\ -2 & 0 & -1 \\ -1 & -1 & 0 \end{pmatrix}, J_y = \begin{pmatrix} 0 & 0 & 1 \\ 0 & 0 & -1 \\ 1 & -1 & 0 \end{pmatrix}. \quad (36)$$

The corresponding band structure of $h_{\text{Dirac}}(\mathbf{k}) = h(\mathbf{K}) + h_{\text{Dirac}}(\mathbf{q})$ is shown in Fig 7, displaying three bands; one of them is a flat band while the other two are dispersive bands with linear spectrum touching at a Dirac point.

Next, we consider the Zeeman term, which is off diagonal both in the spin and sublattice spaces

$$h_{\text{Zeeman}} = - \sum_{i \in A, B, C} \mathbf{M}_i \cdot \mathbf{s} \quad (37)$$

where $\mathbf{s} = (\hbar/2)\boldsymbol{\sigma}$, with $\boldsymbol{\sigma} = (\sigma_x, \sigma_y, \sigma_z)$ the Pauli spin matrices vector. Referring to the spin vectors represented by the arrows in Fig. 6, we have

$$h_{\text{Zeeman}} = -\frac{\hbar}{2} (J_0 \boldsymbol{\sigma}_z M_z + \boldsymbol{\sigma}_\perp \cdot (\mathbf{M}_\perp^A J_A + \mathbf{M}_\perp^B J_B + \mathbf{M}_\perp^C J_C)) \quad (38)$$

where we have added the uniform z part of magnetization; M_z to generalize the formulation to canted spin order (when $M_z = 0$ we recover the coplanar non-collinear spin order) while $\boldsymbol{\sigma}_\perp = (\sigma_x, \sigma_y, 0)$ and $\mathbf{M}_{A\perp} = (M_x^A, M_y^A, 0) = M_\perp (\sqrt{3}/2, -1/2, 0)$ and similarly for the other two sublattices. The J matrices are given by

$$J_0 = \begin{pmatrix} 1 & 0 & 0 \\ 0 & 1 & 0 \\ 0 & 0 & 1 \end{pmatrix}, J_A = \begin{pmatrix} 1 & 0 & 0 \\ 0 & 0 & 0 \\ 0 & 0 & 0 \end{pmatrix}, J_B = \begin{pmatrix} 0 & 0 & 0 \\ 0 & 1 & 0 \\ 0 & 0 & 0 \end{pmatrix}, J_C = \begin{pmatrix} 0 & 0 & 0 \\ 0 & 0 & 0 \\ 0 & 0 & 1 \end{pmatrix}. \quad (39)$$

Defining massive Dirac Hamiltonian

$$h_{\text{MassiveDirac}}(\mathbf{q}) = h(\mathbf{K}) + h_{\text{Dirac}}(\mathbf{q}) + h_{\text{Zeeman}} = h_{\text{Dirac}}(\mathbf{k}) + h_{\text{Zeeman}} \quad (40)$$

which gives the following 6×6 Hamiltonian

$$h_{\text{MassiveDirac}}(\mathbf{q}) = \boldsymbol{\sigma}_0 h(\mathbf{K}) + \frac{\sqrt{3}}{8} t \left(q_x J_x + \sqrt{3} q_y J_y \right) \boldsymbol{\sigma}_0 - \frac{\hbar}{2} (\boldsymbol{\sigma} \cdot \mathbf{M}_J) \quad (41)$$

where $\boldsymbol{\sigma}_0$ is 2×2 identity matrix defined in the spin space and the 3×3 matrix vector \mathbf{M}_J defined in the sublattice space has the following elements

$$\mathbf{M}_J = (M_J^x, M_J^y, M_J^z) = \left(\frac{\sqrt{3}}{2} M_\perp (J_A - J_B), M_\perp \left(J_C - \frac{J_A + J_B}{2} \right), J_0 M_z \right) \quad (42)$$

giving a massive Dirac fermion Hamiltonian, where the mass comes from the Zeeman (last) term in Eq.(41). Diagonalizing the Hamiltonian in the sublattice space, one obtains

$$h_{\text{MassiveDirac}}(\mathbf{q}) \rightarrow h_{\text{MassiveDirac}}^{\text{diag}}(\mathbf{q}) = U^\dagger h_{\text{Dirac}}(\mathbf{k}) U + U^\dagger h_{\text{Zeeman}} U \quad (43)$$

where U is a unitary orthogonal matrix $U^\dagger U = 1$. We choose U to diagonalize the $h(\mathbf{k})$ in the sublattice space, because h_{Zeeman} is already diagonal in this space. Therefore, it is guaranteed that $U^\dagger h_{\text{Zeeman}} U$ remains diagonal in the sublattice space. Doing so, one obtains

$$h_{\text{MassiveDirac}}^{\text{diag}}(\mathbf{q}) = \begin{pmatrix} E_{11}(\mathbf{q}) + V_1 \mathbf{d}^1(\mathbf{q}) \cdot \boldsymbol{\sigma} & 0 & 0 \\ 0 & E_{22}(\mathbf{q}) + V_2 \mathbf{d}^2(\mathbf{q}) \cdot \boldsymbol{\sigma} & 0 \\ 0 & 0 & E_{33}(\mathbf{q}) + V_3 \mathbf{d}^3(\mathbf{q}) \cdot \boldsymbol{\sigma} \end{pmatrix} \quad (44)$$

where $\boldsymbol{\sigma}$ is the Pauli spin matrix vector $\boldsymbol{\sigma} = (\sigma_x, \sigma_y, \sigma_z)$ and $\mathbf{d}^i(\mathbf{q}), i = 1, 2, 3$ is \mathbf{q} -dependent Bloch vector for each state.

The corresponding unit vector $\hat{\mathbf{d}}(\mathbf{q}) = \mathbf{d}(\mathbf{q})/|\mathbf{d}(\mathbf{q})|$ lives on Bloch sphere defined in \mathbf{k} space. The corresponding Hall conductivity can be computed from³

$$\sigma_{xy} = -\frac{1}{8\pi^2} \int_{1\text{BZ}} d^2\mathbf{q} \hat{\mathbf{d}}(\mathbf{q}) \cdot (\partial_{q_x} \hat{\mathbf{d}}(\mathbf{q}) \times \partial_{q_y} \hat{\mathbf{d}}(\mathbf{q})) \equiv \frac{e^2}{2\pi\hbar} C \quad (45)$$

where 1BZ refers to the first Brillouin zone, the partial derivative is in \mathbf{q} space; $\partial_{q_x(q_y)} = \partial/\partial q_{x(y)}$ and we work with the units where $e = \hbar = 1$. The analytical expression for the vector $\mathbf{d}(\mathbf{q})$ is rather complicated as it involves the solution of a cubic polynomial equation, but can in principle be calculated from Eq.(41) with details given in the following paragraphs. It is to be noted that the integral in Eq.(45) resembles the Skyrme number, which simply counts how many times the unit vector $\hat{\mathbf{d}}$ winds around the Bloch sphere in \mathbf{k} space as one sweeps the Brillouin zone. The Chern number can be determined by visualizing the profile of $\hat{\mathbf{d}}$ vector and computing the solid angle it covers as one scans through the \mathbf{q} space. The corresponding Chern number is simply given by $C = S/(4\pi)$, where S is the area (solid angle) covered by the $\hat{\mathbf{d}}$ vector.

The constant prefactor V_i can always be absorbed into the vector $\mathbf{d}^i(\mathbf{q})$, thus giving us freedom to simply set the prefactor to unity. Doing so, the analytical expression for the components of $\mathbf{d}^i(\mathbf{q} = 0)$ vector is found to be, for $i = 1$

$$d_x^1(\mathbf{q} = 0) = \frac{2t^2 \text{Re} \left(\frac{1}{(iM_p^3 - 2t^3 + \sqrt{-M_p^3(M_p^3 + 4it^3)})^{1/3}} \right)}{2 \times 2^{2/3}} + \frac{2\text{Re} \left(\left(iM_p^3 - 2t^3 + \sqrt{-M_p^3(M_p^3 + 4it^3)} \right)^{1/3} \right)}{4 \times 2^{1/3}}; \quad (46)$$

$$d_y^1(\mathbf{q} = 0) = \frac{-2\text{Im} \left[4t^2 \left(\frac{1}{(-iM_p^3 - 2t^3 + \sqrt{-M_p^6 + 4iM_p^3t^3})^{1/3}} \right) \right] - 4 \times 2^{1/3} \text{Im} \left[\left(-iM_p^3 - 2t^3 + \sqrt{-M_p^6 + 4iM_p^3t^3} \right)^{1/3} \right]}{8 \times 2^{2/3}}; \quad (47)$$

$$d_z^1(\mathbf{q} = 0) = -\frac{\hbar M_z}{2} \quad (48)$$

where Re, Im represent the real part and the imaginary part, respectively. Similar expression can be derived for $i = 2, 3$. We have denoted $M_p \equiv M_\perp = \sqrt{M_x^2 + M_y^2}$ which is subject to the constraint $M_z^2 + M_p^2 = M_s^2$ with fixed M_s . Eventually, $d_z^i(\mathbf{q}) = -\hbar M_z/2$ for all $i = 1, 2, 3$, independent of \mathbf{q} . As such, the integral in Eq.(45) can be written explicitly as

$$C = -\frac{1}{4\pi} \int_{1\text{BZ}} d^2\mathbf{q} \hat{d}_z^i(\mathbf{q}) \left(\partial_{q_x} \hat{d}_x^i(\mathbf{q}) \partial_{q_y} \hat{d}_y^i(\mathbf{q}) - \partial_{q_x} \hat{d}_y^i(\mathbf{q}) \partial_{q_y} \hat{d}_x^i(\mathbf{q}) \right) \quad (49)$$

which clearly changes sign when we changes the sign of M_z , noting Eq.(48). In other words, in canted spin order, the Chern number must be an odd function of M_z .

When one tunes the direction of the magnetic moment \mathbf{M}_i from coplanar in the xy plane to collinear along z or vice versa, the band structure deforms dramatically. This is because such reorientation of the direction of the moment amounts to, rather than a small perturbation, a large deformation of the Hamiltonian. The bands are not simply gradually moved away or closer to each other, but rearranged completely. Therefore, it becomes more subtle how to define a gap, starting from the energy eigenvalues of the Hamiltonian. But as described in the main text and as deduced above, the topological properties actually do not depend on the actual size of the gap, but only on its “sign”, which reflects the relative positioning of the bands relative to each other. When

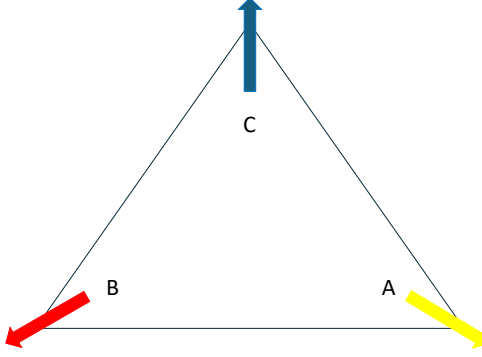


FIG. 6. The unit cell of a kagome lattice with its three sublattices and the corresponding spin vectors.

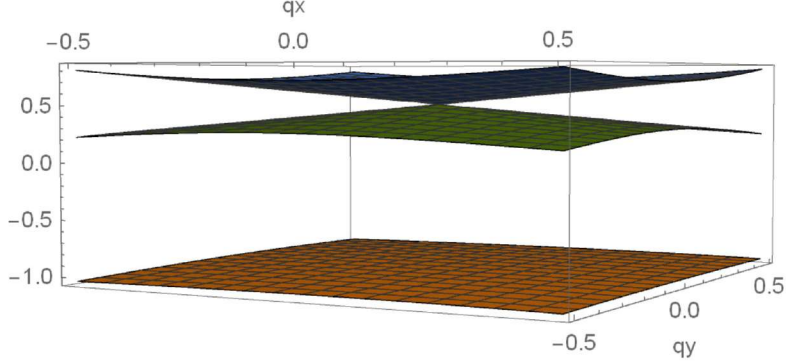


FIG. 7. Band structure of low-energy Hamiltonian $h(\mathbf{K}) + h_{\text{Dirac}}(\mathbf{q})$ with its Dirac point.

the bands get inverted; i.e. when “band inversion” occurs, the topological properties may change. We therefore define the gap Δ by choosing the simplest possible convention; defined in terms of the intra-pair gap,

$$E_g^{\tilde{i}} = E_{\tilde{i}}^+ - E_{\tilde{i}}^- = 2|\mathbf{d}_{\tilde{i}}| \quad (50)$$

where $\tilde{i} = 1, 2, 3$. The gap however must be odd with the change of sign of M_z . So, we define the gap to be

$$\Delta = \text{sign}(M_z) (E_g^{\tilde{i}} - |M_z|) \quad (51)$$

where $|M_z|$ indicates the absolute value of M_z . The profile of this gap is shown in Fig. 8. The main feature of this gap is that it does not change sign as one varies M_z in the northern hemisphere $M_z > 0$ and southern hemisphere $M_z < 0$ of the Bloch sphere; it only changes sign at the equator $M_z = 0$. Note that this gap does not represent the tiny nontrivial gap between nearly-touching bands at the initially Dirac point or quadratic band crossing point. Rather, it represents the gap between spin up and spin down sectors of a given sublattice state, normalized with respect to the z part of Zeeman field M_z . This result predicts that the Chern number remains robust, as long as the gap is non-zero and not overshadowed by any band, as one tune the angle of the canting, and the Chern number changes sign only when the canting passes the equator. This prediction is confirmed numerically in Section III of the Supplementary Materials.

III. ADDITIONAL RESULTS

A. The Role of Onsite Energies: Switch of Topological Phase Transition

Onsite energies can be used as a switch to split the $C = \pm 5$ Chern peaks into different series of lower Chern number peaks. This is illustrated in Fig. 10 where two different Chern series, the so-called 1-2-2 series and 3-2 series are obtained by judiciously setting the onsite energies to have corresponding degeneracies. In a sense, the onsite energy can therefore be regarded as a

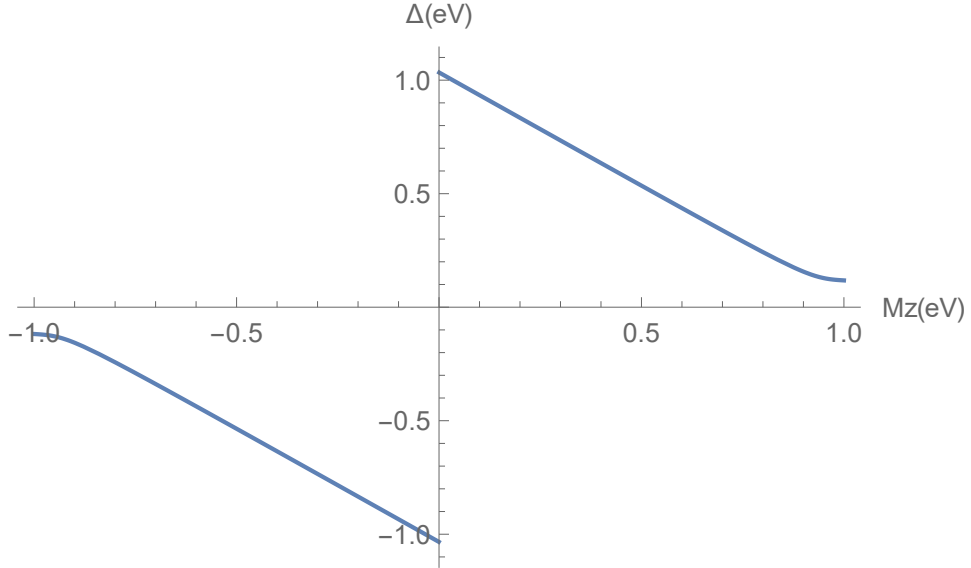


FIG. 8. The dependence of the gap Δ on M_z . Parameters used are $t = -0.25\text{eV}$, $M_s = 1.0\text{eV}$ where $M_z = M_s \cos \theta$.

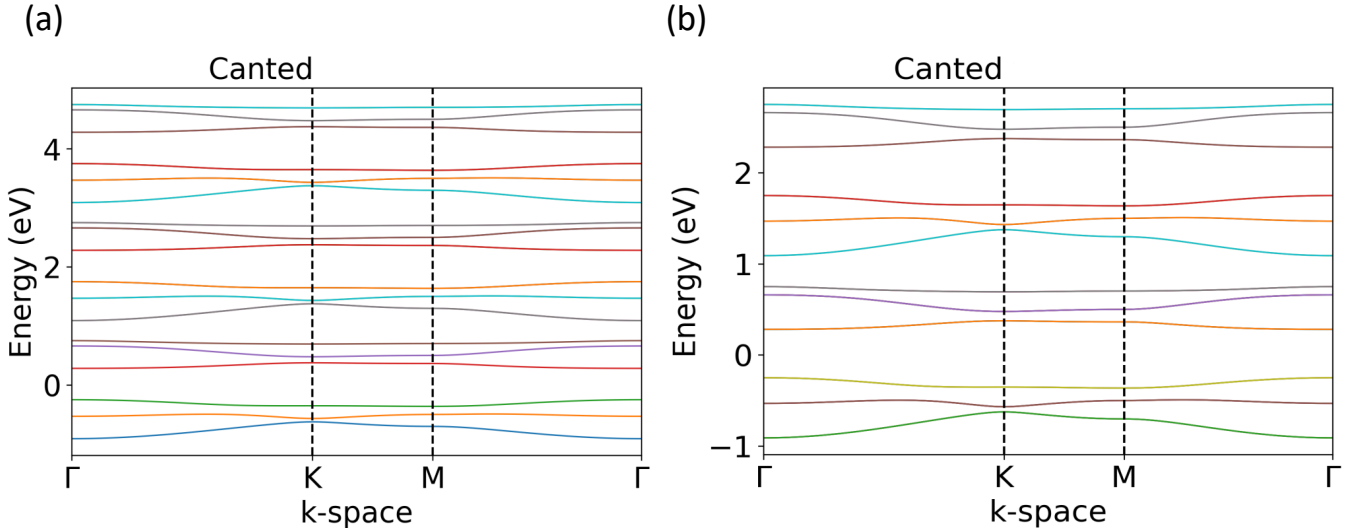


FIG. 9. Electronic band structures for non-coplanar (canted) non-collinear spin orders at $\theta = 53^\circ$ and $M_s = 1.0\text{eV}$ with isotropic Slater-Koster integrals $V_{dd\sigma} = V_{dd\delta} = V_{dd\pi} = -0.25\text{eV}$ and different onsite energies: (a) $E_z^2 = 0.0\text{eV}$, $E_{xz,yz} = 2.0\text{eV}$, and $E_{xy,x^2-y^2} = 4.0\text{eV}$ and (b) $E_z^2 = 0.0\text{eV}$, $E_{xz,yz} = 2.0\text{eV}$, and $E_{xy,x^2-y^2} = 0.0\text{eV}$.

switch of a topological phase transition that changes the Chern number of the quantum anomalous Hall state, corresponding to the number of chiral edge states present at a given Fermi energy. So far, we have assumed degeneracy in terms of onsite energy for d -orbitals of the same symmetry; between d_{xz} and d_{yz} orbitals, and also between d_{xy} and $d_{x^2-y^2}$ orbitals. In the most general case, these orbitals are not necessarily degenerate in onsite energy; their onsite energies are split, which can be caused by orbital rotation due to crystal field splitting for example. We reserve this more complicated case for future work.

B. Robustness of $|C| = 5$ QAHE with Anisotropy in Slater-Koster Integrals

In the main text, we have presented results mainly based on our model assuming isotropic Slater-Koster integrals. This is a very idealized situation; in real materials, Slater-Koster integrals that would fit first-principle band structure would in general be anisotropic. Question naturally arise whether the predicted results coming from isotropic limit would be applicable to any real materials.

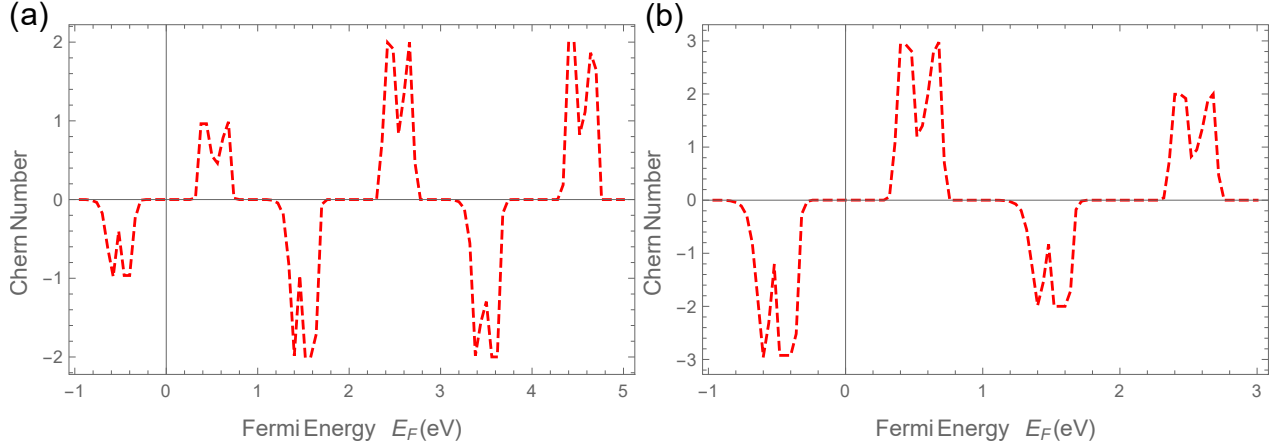


FIG. 10. The dependence of the Chern number C on the Fermi energy E_F (eV) at $T = 0.0001\text{eV} (= 1.1\text{K})$ for kagome d -electron system with 120° canted (non-coplanar) antiferromagnetic order, with well separated onsite energies (a) $E_1 = 0.0\text{eV}$, $E_2 = 2.0\text{eV}$, and $E_3 = 4.0\text{eV}$, giving a set of plateaus with $C = \pm 1, \pm 2$. A different set of parameters (b) $E_1 = 0.0\text{eV}$, $E_2 = 2.0\text{eV}$, and $E_3 = 0.0\text{eV}$ gives a series of Chern numbers $C = \pm 3, \pm 2$.

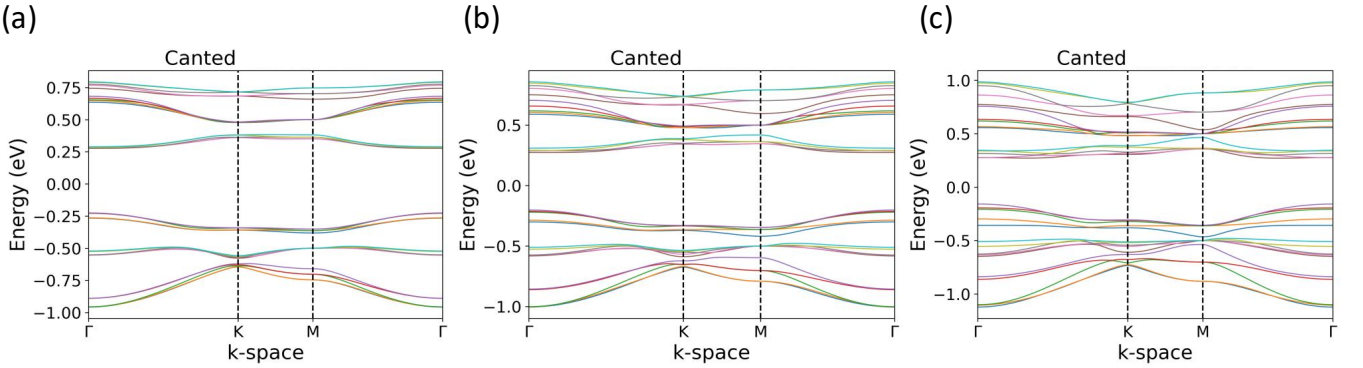


FIG. 11. Electronic band structures for non-coplanar (canted) non-collinear spin orders and anisotropic Slater-Koster integrals by: (a) 20%; $V_{dd\pi} = -0.25\text{eV}$, $V_{dd\delta} = -0.30\text{eV}$, $V_{dd\sigma} = -0.20\text{eV}$, (b) 50% $V_{dd\pi} = -0.25\text{eV}$, $V_{dd\delta} = -0.375\text{eV}$, $V_{dd\sigma} = -0.125\text{eV}$, and (c) 80% $V_{dd\pi} = -0.25\text{eV}$, $V_{dd\delta} = -0.45\text{eV}$, $V_{dd\sigma} = -0.05\text{eV}$, all of which without SOC and with equal onsite energies set to zero. In (a), all the four nontrivial gaps survive, while in (b) and (c), only two of the four of them survive; the other two get overlapped by bands.

To answer this question, we hereby present the result of test calculations with anisotropic Slater-Koster integrals. The band structures for different cases with canted spin order but with different amounts of anisotropy in the Slater-Koster integrals are presented in Fig. 11. Starting from $V_{dd\pi} = V_{dd\delta} = V_{dd\sigma} = -0.25\text{eV}$ in the isotropic limit, with clear $C = \pm 5$ Chern peaks, we make the V_{dd} 's anisotropic by (a) 20%; $V_{dd\pi} = -0.25\text{eV}$, $V_{dd\delta} = -0.30\text{eV}$, $V_{dd\sigma} = -0.20\text{eV}$, (b) 50% $V_{dd\pi} = -0.25\text{eV}$, $V_{dd\delta} = -0.375\text{eV}$, $V_{dd\sigma} = -0.125\text{eV}$, and (c) 80% $V_{dd\pi} = -0.25\text{eV}$, $V_{dd\delta} = -0.45\text{eV}$, $V_{dd\sigma} = -0.05\text{eV}$. The resulting Chern number is presented in Fig. 12, indicating that the predicted large Chern number is robust even against relatively strong anisotropy in the Slater-Koster integrals; the large Chern number $C = \pm 5$ can thus occur in real materials, where the Slater-Koster integrals normally very anisotropic, as long as the nontrivial gaps remain. The only downside of anisotropic Slater-Koster integrals is that such nontrivial gaps become much narrower, as attested in Fig. 11, making it harder to fine tune the Fermi energy (filling factor or electron density) to realize the coveted large Chern quantum anomalous Hall effect.

C. Dependence of Chern Number C on Canting Angle

The Chern number turns out to be robust with respect to the canting angle. The profiles of the band structure and the corresponding Chern number vs. Fermi energy for a set of six canting angles are shown respectively in Figs. 13 and 14. In

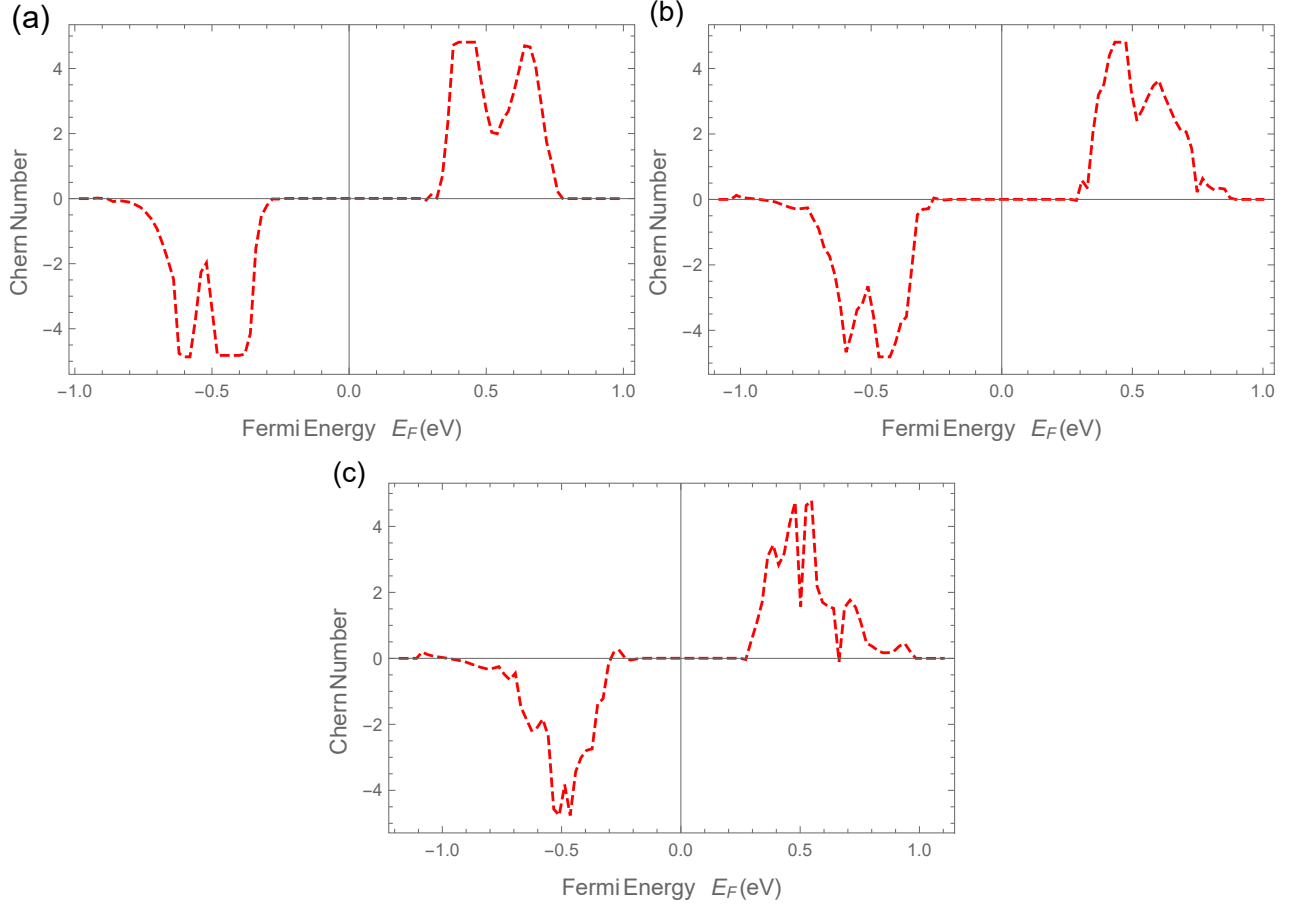


FIG. 12. The dependence of the Chern number C on the Fermi energy E_F (eV) at $T = 0.0001\text{eV} (= 1.1\text{Kelvin})$ for kagome d -electron system with 120° canted (non-coplanar) antiferromagnetic order, with anisotropic Slater-Koster integrals (top, 20% anisotropy), still giving the same set of record-breaking value of large Chern number $C = \pm 5$. Stronger anisotropy by 50% (middle) and 80% (bottom) reconfigures the Chern number profile entirely with still visible peaks at $C = \pm 5$ (up to the attainable numerical convergence), despite much narrower energy bandwidth.

all these cases, the Chern peaks with $|C| = 5$ exist. This finding is easy to explain. As shown in⁴, in an electron model on kagome lattice with the flux Φ in triangle, the resulting Chern number characterizing quantum anomalous Hall effect only depends on the sign of the flux; $C = \text{sign}[\sin(\Phi)]$. As such, the actual value of the flux (related to the canting angle Θ) as given by Eq.(2) in the main text, does not really matter; as long as it is neither zero nor π , the Chern number (from each of the d orbital) would be nonzero $C = \pm 1$.

¹W. A. Harrison, *Electronic Structure and the Properties of Solids: The Physics of the Chemical Bond* (Dover Publications, Inc., New York (1980)).

²I. Makhfudz, M. Cherkasskii, M. Alipourzadeh, Y. Hajati, P. Lombardo, S. Schäfer, S. V. Kusminskiy, and R. Hayn, Quantum anomalous Hall effect in d -electron kagome systems: Chern insulating states from transverse spin-orbit coupling, *Phys. Rev. B* 110, 235130 (2024).

³Qi, X. L., Wu, Y.-S., and Zhang, S.-C., Topological quantization of the spin Hall effect in two-dimensional paramagnetic semiconductors, *Phys. Rev. B* 74, 085308 (2006).

⁴Ohgushi K., Murakami S., Nagaosa N., Spin Anisotropy and Quantum Hall Effect in the Kagome Lattice - Chiral Spin State based on a Ferromagnet, *Phys. Rev. B* 62, R6065 (2000).

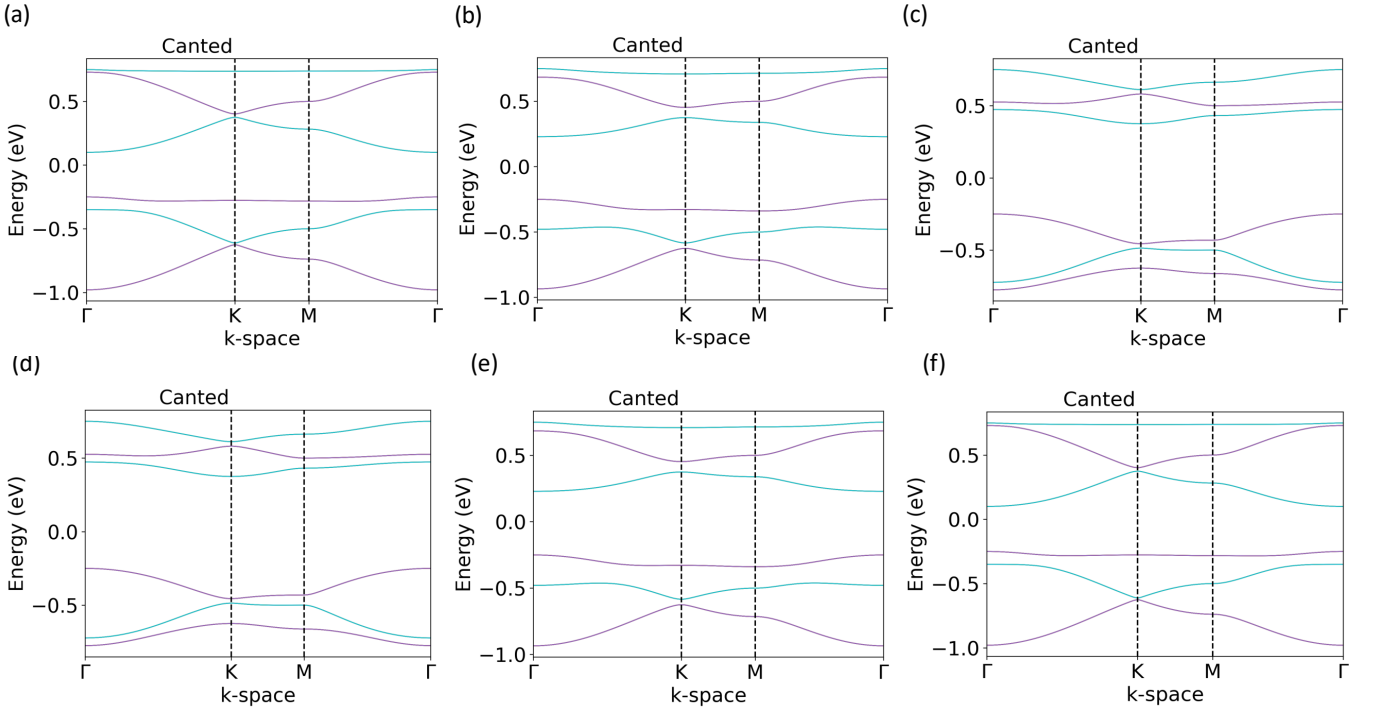


FIG. 13. Electronic band structures for non-coplanar (canted) non-collinear spin orders and isotropic Slater-Koster integrals V , but with different canting angle: (a) $\theta = 15^\circ$,(b) $\theta = 45^\circ$,(c) $\theta = 85^\circ$,(d) $\theta = 95^\circ$,(e) $\theta = 135^\circ$, and (f) $\theta = 165^\circ$, all of which without SOC and with equal onsite energies set to zero.

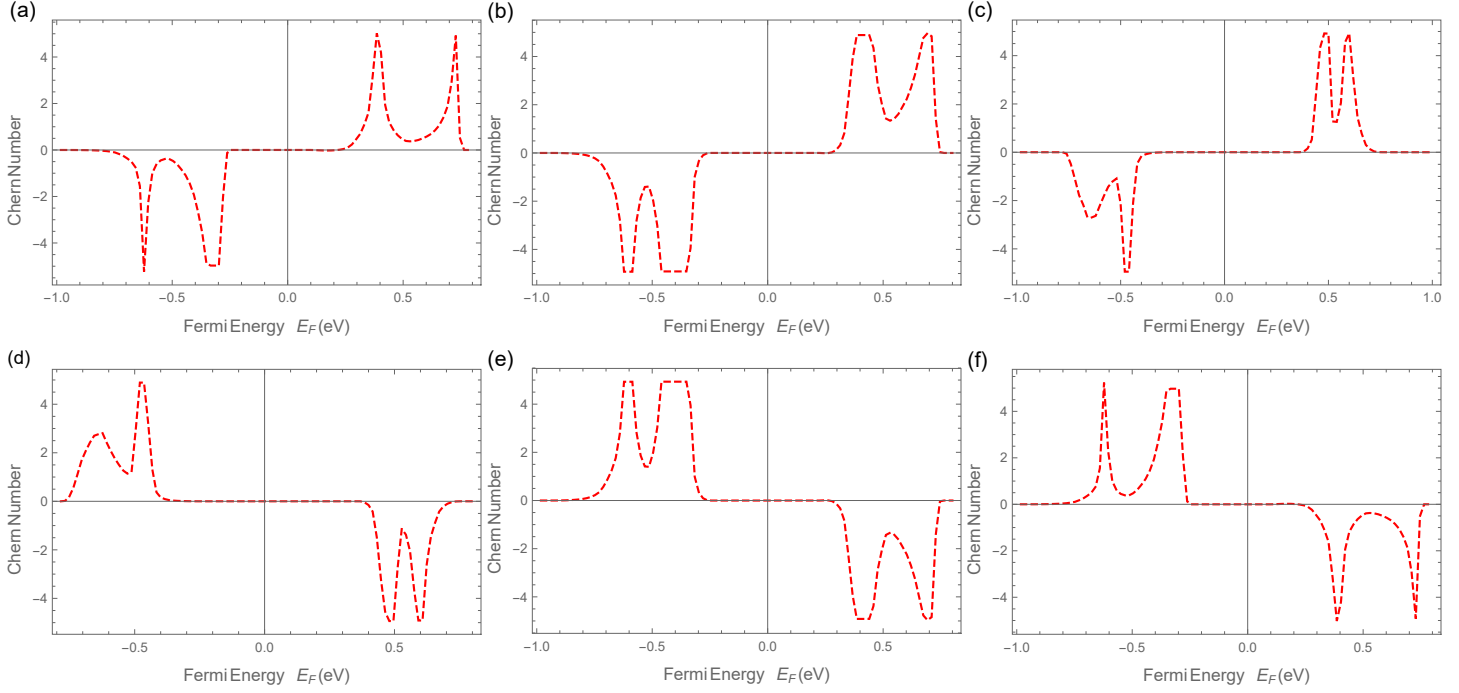


FIG. 14. The dependence of the Chern number C on the Fermi energy E_F (eV) at $T = 0.0001\text{eV} (= 1.1\text{Kelvin})$ for kagome d -electron system with 120° canted (non-coplanar) antiferromagnetic order, on the canting angle with (a) $\theta = 15^\circ$, (b) $\theta = 45^\circ$, (c) $\theta = 85^\circ$, (d) $\theta = 95^\circ$, (e) $\theta = 135^\circ$, and (f) $\theta = 165^\circ$ (measured from z axis), while $M_s = \sqrt{M_x^2 + M_y^2 + M_z^2} = 1.0\text{eV}$ is fixed, still giving the same set of record-breaking value of large Chern number $C = \pm 5$.